

# Effective Equations for Discrete Systems: A Time Stepper Based Approach

Joakim Möller\*    Olof Runborg\*    Panayotis G. Kevrekidis<sup>†</sup>  
Kurt Lust<sup>‡</sup>    Ioannis G. Kevrekidis<sup>§</sup>

November 20, 2018

## Abstract

We propose a computer-assisted approach to studying the effective continuum behavior of spatially discrete evolution equations. The advantage of the approach is that the “coarse model” (the continuum, effective equation) need not be explicitly constructed. The method only uses a time-integration code for the discrete problem and judicious choices of initial data and integration times; our bifurcation computations are based on the so-called Recursive Projection Method (RPM) with arc-length continuation (Shroff and Keller, 1993). The technique is used to monitor features of the genuinely discrete problem such as the pinning of coherent structures and its results are compared to quasi-continuum approaches such as the ones based on Padé approximations.

**Mathematical Subject Classification.** 65P30, 74Q99, 37L60, 37L20, 39A11.

## 1 Introduction

In contemporary science and engineering modeling many situations arise in which the physical system consists of a lattice of discrete interacting units. The role of discreteness in modifying the behavior of solutions of continuum non-linear PDEs has recently been increasingly appreciated. The relevant physical contexts can be quite diverse, ranging from the calcium burst waves in living cells [1] to the propagation of action potentials through the tissue of the cardiac

---

\*Department of Numerical Analysis and Computer Science, KTH, 10044 Stockholm, Sweden.

<sup>†</sup>Department of Mathematics and Statistics, University of Massachusetts, Amherst, MA 01003 USA.

<sup>‡</sup>Departement Computerwetenschappen, Katholieke Universiteit Leuven, Celestijnenlaan 200A, B-3001 Heverlee, Belgium.

<sup>§</sup>Department of Chemical Engineering, Program for Applied and Computational Mathematics, Department of Mathematics, Princeton University, Princeton, NJ 08544, USA.

cells [2] and from chains of chemical reactions [3] to applications in superconductivity and Josephson junctions [4], nonlinear optics and waveguide arrays [5], complex electronic materials [6], the dynamics of neuron chains or lattices [7, 8] or the local denaturation of the DNA double strand [9].

Whether the phenomenon in question is the propagation of an excitation wave along a neuron lattice, the electric field envelope in an optical waveguide array, or the behavior of a tissue consisting of an array of individual cells, we would often like to model the system through a “coarse level” effective continuum evolution equation that retains the essential features of the actual (discrete) problem. Typically computational modeling of such systems involves two steps: the derivation of effective continuum equations, followed by their analysis through traditional numerical tools. In this paper we attempt to circumvent the derivation of explicit (closed) continuum effective equations, and analyze the effective behavior directly. This is accomplished through short, appropriately initialized simulations of the detailed discrete process, a procedure that we call the “coarse time stepper”. These simulations provide estimates of the quantities (residuals, action of Jacobians, time derivatives, Fréchet derivatives) that would be directly evaluated from the effective equation, had such an equation been available. The estimated quantities are processed by a higher level numerical procedure (in this case, the Recursive Projection Method, RPM, of Shroff and Keller [10]) which computes the effective, macroscopic behavior (in this case, traveling waves and their coarse bifurcations). A more general discussion of the combination of coarse time stepping with continuum numerical techniques beyond RPM can be found in [11]. We have recently demonstrated such an approach to the computation of the effective behavior (in some sense, homogenization) of spatially heterogeneous problems [12]. This paper constitutes an extension of this idea to spatially discrete problems.

The paper is organized as follows: we begin with a brief review of the coarse time stepper for spatially discrete problems. We then discuss our illustrative problem (a front for a discrete reaction-diffusion system) and its properties. A description of our implementation of the coarse time stepper for the bifurcation analysis of this particular problem is then presented, followed by numerical results. We conclude with a discussion of an alternative approach that involves the derivation of an explicit effective evolution equation (based on Padé approximations), and of the scope and applicability of our method.

## 2 A Coarse Time Stepper for Discrete Systems

Consider a discrete system where each unknown is associated with a point on a lattice in space. In the discussion here, we consider a one-dimensional regular lattice for simplicity. Higher dimensional and/or possibly irregular, lattices can be treated in a similar way. We denote the unknowns  $\{u_\ell\}$ , with  $\ell \in \mathbb{Z}$ , and the corresponding points  $\{x_\ell\}$ , such that  $x_\ell = \ell\Delta x$ , where  $\Delta x$  is the lattice spacing.

We assume that the system is governed by the ordinary differential equations

$$\frac{du_\ell}{dt} = F(t, u_{\ell-n}, \dots, u_{\ell+n}), \quad \ell \in \mathbb{Z}, \quad (1)$$

where  $n > 0$  is an integer representing the range of interaction between lattice points. We want to describe this discrete system dynamics through a continuous function  $v(t, x)$  that models the “coarse” behavior of the unknowns on the lattice:

$$u_\ell(t) \approx v(t, x_\ell), \quad \forall t, \ell,$$

in some appropriate sense. We denote  $v$  the *coarse continuous solution* of (1) and we assume that  $n$  is not large and that there exists an effective, spatially continuous evolution equation for  $v(x, t)$  of the form

$$v_t = P(t, v, \partial_x v, \dots, \partial_x^M v), \quad (2)$$

for some  $P$  and integer  $M$ . Such an effective equation for  $v$  should “average over” the detailed discrete structure of the medium; if there are no macroscopic variations of the discrete medium, this equation should therefore be translationally invariant; for the moment, we will confine ourselves to this case. In terms of (1), we can express this as: if  $F$  does not depend on  $\ell$ , and if  $v$  and  $\tilde{v}$  are two solutions to the effective equation (2) satisfying  $v(0, x) = \tilde{v}(0, x + s)$  for all  $x$ , then  $v(t, x) = \tilde{v}(t, x + s)$  for all time  $t > 0$ , all  $x$ , and all shifts  $s$ .

It is interesting to consider what the result of integrating such an effective equation with a particular, continuum initial condition  $v_0(x)$ , would physically mean. There clearly exists an uncertainty in how such a continuum initial condition would be imparted to (sampled by) the lattice. One way would be to set  $u_\ell(0) = v_0(x_\ell)$ , for all  $\ell$ , but we could equally well set  $u_\ell(0) = v_0(x_\ell + s)$  for any  $s \in [0, \Delta x)$ . There exists, therefore, a one-parameter uncertainty parametrized by a continuous shift  $s$ . Simulations resulting from different lattice samplings of the same continuum initial condition could be quite different. This is best illustrated by thinking of a single-peaked function as the continuum initial condition: the peak may lie precisely at a lattice point, or could fall in-between lattice points. It is reasonable to consider as a useful effective continuum equation one which takes into account all possible shifts of the initial condition within a cell; in analogy with our earlier work [12], we would like to analyze an effective equation that would describe the expected result—taken over all possible shifts—of sampling the initial condition by the lattice.

We will use the coarse time stepper approach to simulate an effective equation like (2). In this setting, we approximate  $v(t, x)$  by the coarse time stepper solution  $\tilde{u}(t, x)$  at discrete times  $nT$ , where  $T$  is the *time horizon* of the coarse time stepper. Using the terminology of this framework, we do the following steps, starting from a continuous initial condition  $v_0(x) = \tilde{u}(0, x)$ .

- *Lifting.* This initial data  $v_0(x)$  is “lifted” to an ensemble of  $N_c$  different initial states of (1) by sampling,

$$u_\ell^j(0) = v_0(x_\ell + j\Delta s), \quad \Delta s = \Delta x/N_c, \quad j = 0, \dots, N_c - 1. \quad (3)$$

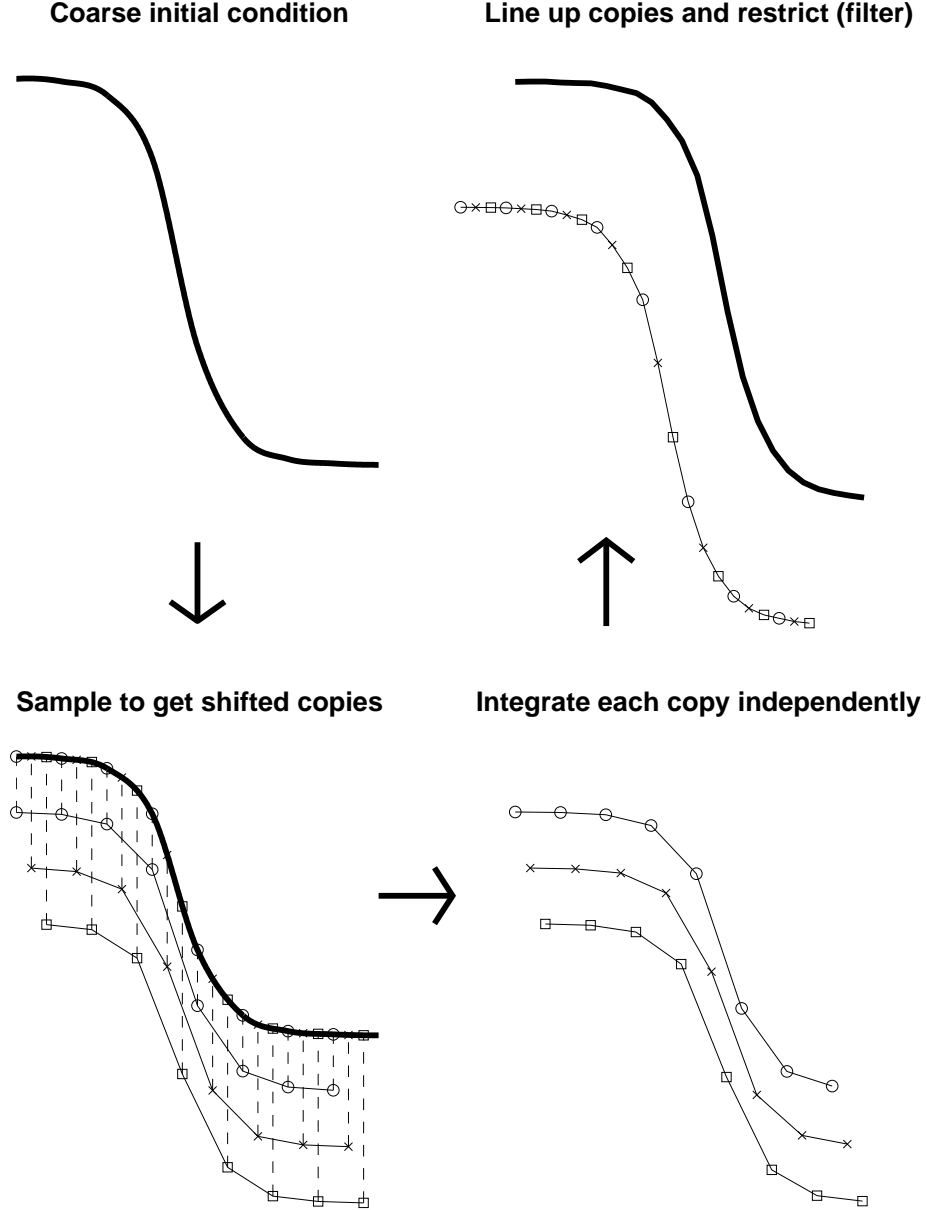


Figure 1: The coarse time stepper: Starting from a coarse initial condition  $v_0(x)$ , lift it by sampling to an ensemble of initial data,  $\{u_j(0)\}$ ,  $j = 0, \dots, N_c - 1$ , for the system and evolve each set for time  $T$ . Line up solutions at time  $T$  and interpolate to get  $\bar{u}(x)$ . Finally, filter  $\bar{u}(x)$  to get  $\tilde{u}(T, x)$ , the result of the coarse time stepper at  $t = T$ .

Setting  $\mathbf{u}_j = \{u_\ell^j\}$ , we write this symbolically as

$$\mathbf{u}_j(0) = \mu_j v_0,$$

where  $\{\mu_j\}$  are called the lifting operators. In this case they simply sample a continuous function.

- *Evolve.* Each ensemble of initial data is evolved till time  $T$  according to the “true dynamics” (1),

$$\mathbf{u}_j(T) = \mathcal{T}_T \mathbf{u}_j(0), \quad j = 0, \dots, N_c - 1. \quad (4)$$

where  $\mathcal{T}_\tau$  is the solution operator of (1) evolving  $\mathbf{u}(t)$  to  $\mathbf{u}(t + \tau)$ . This step thus generates an ensemble of solutions  $\mathbf{u}_j(T)$  at time  $T$ .

- *Restrict.* Via the restriction operator  $\mathcal{M}$ , the ensemble of solutions is brought back to a continuous function.

$$\tilde{u}(T, x) = \mathcal{M}\{\mathbf{u}_j(T)\}, \quad j = 0, \dots, N_c - 1. \quad (5)$$

To ensure consistency we require that  $\mathcal{M}\{\mu_j\} = I$ . The restriction operator  $\mathcal{M}$  is typically defined as follows. The solutions  $\mathbf{u}_j(T)$  are thought of as sample values of a function  $\bar{u}$  such that  $\bar{u}(x_\ell + j\Delta s) = u_\ell^j$ . The function  $\bar{u}$  is recovered by interpolating the sample values and the restriction  $\tilde{u}(x, T) = \mathcal{M}\{\mathbf{u}_j(T)\}$  is finally given as a coarse scale filtering of  $\bar{u}(x)$ .

These steps are illustrated in Figure 1. For  $n > 0$  we define  $\tilde{u}(nT, x)$  recursively by applying the same construction. Hence,

$$\tilde{u}(nT, x) = \mathcal{M}\{\mathcal{T}_T \mu_j\} \tilde{u}((n-1)T, x). \quad (6)$$

The hope is that the coarse time stepper solution  $\tilde{u}(nT, x)$ , at these discrete points in time, can be obtained from a closed evolution equation like (2) whose solution,  $v(t, x)$  (defined for all  $t$ ), agrees, at least approximately, with the coarse solution obtained from the procedure above, at the discrete points in time,  $v(nT, x) \approx \tilde{u}(nT, x)$ . We will refer to the procedure as the *coarse time stepper*.

In order to approximate  $v$  numerically, we must use a finite representation of  $\tilde{u}(nT, x)$ . We let  $\mathbf{v}^n = \{v_k^n\}_{k=0}^{M-1}$ , be this representation at time  $t = nT$ . The elements  $\{v_k^n\}$  could be nodal values, cell averages or, more generally, coefficients for finite elements or other basis functions. Let  $\Pi$  be the operator realizing the function from the finite representation,  $(\Pi \mathbf{v}^n)(x) = \tilde{u}(nT, x)$ . We also require that the restriction operator projects on the subspace spanned by the finite representation, and we can redefine it to also convert the projected function to this representation. Symbolically, we then write the coarse time stepping

$$\mathbf{v}^{n+1} = \mathcal{M}\{\mathcal{T}_T \mu_j\} \Pi \mathbf{v}^n =: G(\mathbf{v}^n). \quad (7)$$

Note that we may not be able to write down the explicit expression for  $G$  or the equation (2) for  $v(t, x)$ , but our definition of  $\tilde{u}(t, x)$  allows us to realize its time- $T$  map numerically in a straightforward fashion.



### 3 A Discrete Traveling Front Example

The effects of discreteness on the propagation of traveling wave solutions have been documented and analyzed in many different settings over the last two decades. From the pinning of travelling waves in discrete arrays of coupled torsion pendula and Hamiltonian models [14, 15], to the trapping of coherent structures in dissipative lattices of coupled cells [16, 17] (see also references therein), the role of spatial discreteness has triggered a large interest in a diverse host of settings.

Effective equations capable of describing the nature of the solutions of discrete problems should successfully capture the effects of discreteness on the traveling wave shape and speed. More importantly, they should be capable of accurately predicting qualitative transitions (bifurcations) that are *inherently due to the discreteness*. The most prominent of those is probably the pinning of traveling waves and fronts often observed when the lattice spacing becomes sufficiently large. To illustrate the performance of our proposed coarse equation in capturing such a front pinning, we have chosen what is arguably a prototypical spatially discrete problem capable of exhibiting it: a one-dimensional lattice with scalar bistable on-site kinetics and nearest neighbor diffusive coupling between lattice sites. Our test problem is, therefore, a discrete reaction–diffusion system described by

$$\frac{du_\ell}{dt} = \frac{1}{(\Delta x)^2}(u_{\ell-1} - 2u_\ell + u_{\ell+1}) + f(u_\ell), \quad \ell \in \mathbb{Z} \quad (8)$$

with

$$f(u) = 2u(u-1)(\eta-u), \quad \eta = 0.45. \quad (9)$$

This can serve as a model of e.g. individual cells in the cardiac tissue which are resistively coupled through gap junctions (see e.g., [16] and references therein). In this case the solution  $u_\ell$ , would correspond to the electrical potential of the cells. For small  $\Delta x$  the system possesses solutions that can be characterized as *discrete traveling fronts*: see Figure 4. These solutions have a near constant shape and travel in a “lurching” manner. When  $\Delta x$  becomes sufficiently large, front propagation fails (front pinning). In our example, this happens at  $\Delta x = \Delta x^* \approx 2.3$ , see Figure 3. The front speed for an infinite lattice approaches the asymptotic “PDE speed” value 0.1 as the lattice size tends to zero.

We will examine how faithful the coarse time stepper is to the properties of the solutions of the full discrete model (8). Our numerical simulations are restricted to a finite domain, using  $N = 64$  grid points. At the boundaries, we prescribe Neumann-type conditions

$$\begin{aligned} u_N - u_{N-1} &= 0, \\ u_0 - u_{-1} &= 0. \end{aligned}$$

This should model the full problem accurately as long as the (relatively narrow) front is positioned sufficiently far from the boundary.

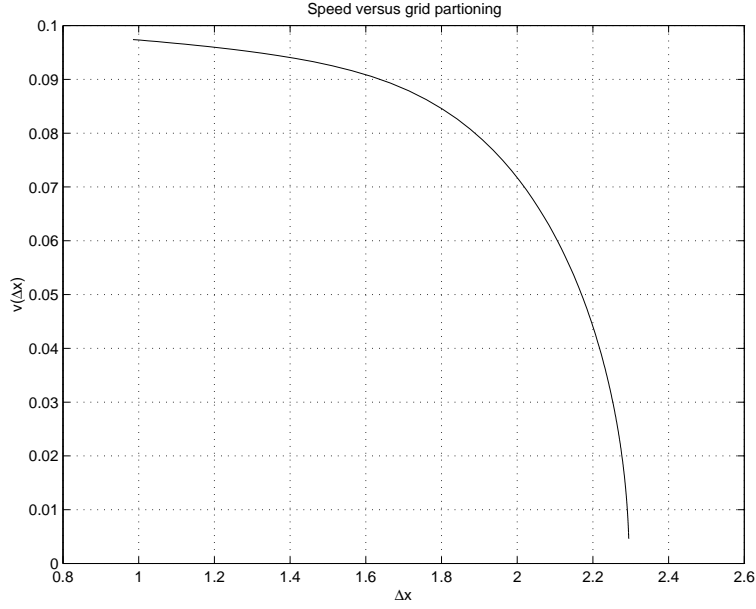


Figure 3: The speed of the front as a function of  $\Delta x$ . As the lattice spacing is increased, the speed  $v$  approaches zero; the front stops at  $\Delta x^* \approx 2.3$ .

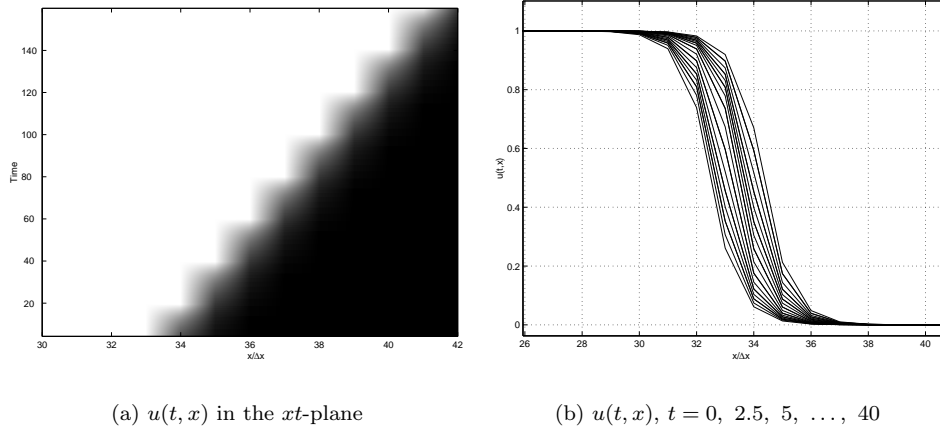


Figure 4: The plot illustrates how the front advances when  $\Delta x = 1.75$ . The left figure shows the front in the  $xt$ -plane; the grayscale is proportional to the solution  $u(t, x)$ . The right figure shows the solution as a function of  $x$  at different time levels. The time interval is  $t \in [0, 40]$ . Looking at the spacing between the solution instances, we can see how the front speed varies in a lurching manner.



### 3.1 Construction of the coarse time stepper

In this section we detail the procedures associated with the coarse time stepper applied to the test problem (8, 9) on the finite interval  $I = [0, L]$ , where  $L = N\Delta x$  and the cell locations are  $x_j = j\Delta x$ , with  $j = 0, \dots, N-1$ .

Our choice of finite representation of the coarse solution are  $M$  nodal values  $\mathbf{v}^n = \{v_k^n\}$ ,  $k = 0, \dots, M-1$ , evaluated at  $t = nT$  and  $y_k = k\Delta y$ , with  $M\Delta y = N\Delta x$ .

For many solution shapes Fourier interpolation would be a natural interpolation operator realizing the coarse solution  $\tilde{u}(nT, x)$  from  $\mathbf{v}^n$ . We denote direct Fourier interpolation by  $\Pi^f$ . We could then define the corresponding lifting operators  $\mu_j^f$  via the *shifting* operator  $\mathcal{S}_s^f : \mathbb{R}^M \rightarrow \mathbb{R}^N$ ,

$$\mu_j^f \mathbf{u} := \mathcal{S}_{j\Delta s}^f \mathbf{u}, \quad (\mathcal{S}_s^f \mathbf{u})_\ell := (\Pi^f \mathbf{u})(x_\ell + s), \quad s \geq 0,$$

where  $\Pi^f$  uses  $\{y_k\}$  as interpolation nodes. In our case, however, the solution is not periodic on  $I$  and we get large errors if we use  $\mathcal{S}_s^f$  directly. Instead we apply Fourier interpolation to the *differences* of the  $\mathbf{v}^n$  sequence. We thus use the modified shifting operator  $\mathcal{S}_s : \mathbb{R}^M \rightarrow \mathbb{R}^N$  given by

$$\mathcal{S}_s \mathbf{u} := C\mathcal{S}_s^f D, \quad (C\mathbf{u})_\ell := 1 + \sum_{j=0}^{\ell} u_j, \quad (D\mathbf{u})_\ell := \begin{cases} u_0 - 1, & \ell = 0, \\ u_\ell - u_{\ell-1}, & \ell > 0. \end{cases} \quad (10)$$

We then define the lifting operator  $\mu : \mathbb{R}^M \rightarrow \mathbb{R}^{N \times N_c}$  (acting directly on  $\mathbf{v}^n$ ) as

$$\mu \mathbf{v}^n = \{\mu_j \mathbf{v}^n\}, \quad \mu_j \mathbf{v}^n := \mathcal{S}_{j\Delta s} \mathbf{v}^n, \quad \Delta s = \frac{\Delta y}{N_c},$$

where  $j = 0, \dots, N_c - 1$ .

The restriction operator  $\mathcal{M} : \mathbb{R}^{N \times N_c} \rightarrow \mathbb{R}^M$  is also defined using the shifting operators, but now with negative shifts,

$$\mathcal{S}_{-s}^f : \mathbb{R}^N \rightarrow \mathbb{R}^M, \quad (\mathcal{S}_{-s}^f \mathbf{u})_k := (\Pi^f \mathbf{u})(y_k - s), \quad s \geq 0,$$

where  $\Pi^f$  uses  $\{x_\ell\}$  as interpolation nodes. We then set  $\mathcal{S}_{-s} = C\mathcal{S}_{-s}^f D$  and let

$$\mathcal{M}\{\mathbf{u}_j\} := \frac{1}{N_c} \sum_{j=0}^{N_c-1} \mathcal{S}_{-j\Delta s} \mathbf{u}_j.$$

Note that these choices of  $\mu$  and  $\mathcal{M}$  are consistent when  $N \geq M$ . Then, by the sampling theorem  $\mathcal{S}_{-s}^f \mathcal{S}_s^f = I$  on  $\mathbb{R}^M$ . Moreover, it is easy to see that  $CD = DC = I$ . Therefore, we also have

$$\mathcal{S}_{-s} \mathcal{S}_s = C\mathcal{S}_{-s}^f D C \mathcal{S}_s^f D = C\mathcal{S}_{-s}^f \mathcal{S}_s^f D = CD = I,$$

on  $\mathbb{R}^M$  and consequently,

$$\mathcal{M} \mu \mathbf{v}^n = \frac{1}{N_c} \sum_{j=0}^{N_c-1} \mathcal{S}_{-j\Delta s} \mu_j \mathbf{v}^n = \frac{1}{N_c} \sum_{j=0}^{N_c-1} \mathcal{S}_{-j\Delta s} \mathcal{S}_{j\Delta s} \mathbf{v}^n = \frac{1}{N_c} \sum_{j=0}^{N_c-1} \mathbf{v}^n = \mathbf{v}^n.$$

We should also remark here that, in the special case when  $N = M$ , we have

$$\left( \frac{1}{N_c} \sum_{j=0}^{N_c-1} \mathcal{S}_{-j\Delta s}^f \mathbf{u}_j \right)_\ell = (P_N \Pi^f \bar{\mathbf{u}})(x_\ell), \quad \bar{\mathbf{u}} = \{\bar{u}_r\}, \quad \bar{u}_{\ell+jN} = u_\ell^j,$$

where  $P_N$  is a projection on the  $N$  lowest Fourier modes. Hence, if we used direct Fourier interpolation and  $M = N$ , then our definition of  $\mathcal{M}$  is equivalent to lowpass filtering of  $\bar{\mathbf{u}}$ , the lined up copies described in Figure 1, top right. When we replace  $\mathcal{S}_s^f$  by  $\mathcal{S}_s$  we do not retain exactly this property, and a definition of  $\mathcal{M}$  based on simple lowpass filtering is no longer consistent. However, our procedure still corresponds to a type of lowpass filtering, although a more complicated one.

For the time integration of (8) we use the Crank–Nicolson method, treating the nonlinear term explicitly. Thus, with  $\mathbf{w}^0 = \{w_\ell^0\} \in \mathbb{R}^N$ ,

$$\mathcal{T}_T \mathbf{w}^0 := \mathbf{w}^{N_T} = \{w_\ell^{N_T}\}, \quad N_T \Delta t = T,$$

where  $\{w_\ell^n\}$  are given iteratively by

$$\begin{aligned} w_\ell^{n+1} - \frac{\Delta t}{2(\Delta x)^2} (w_{\ell-1}^{n+1} - 2w_\ell^{n+1} + w_{\ell+1}^{n+1}) \\ = w_\ell^n + \frac{\Delta t}{2(\Delta x)^2} (w_{\ell-1}^n - 2w_\ell^n + w_{\ell+1}^n) + \Delta t f(w_\ell^n), \end{aligned}$$

for  $\ell = 0, \dots, N-1$ , together with the free boundary conditions

$$\begin{aligned} w_{-1}^n - w_0^n &= 0, \\ w_N^n - w_{N-1}^n &= 0. \end{aligned}$$

In our computations we use the time step  $\Delta t = 0.01$ .

### 3.2 Steady state formulation

The coarse solution  $\tilde{u}(nT, x)$  as we have defined it is a (practically) constant shape moving front. In order to convert this moving state into a stationary state, we can factor out the movement through a procedure based on *template fitting* ([18, 12], see also [19]) which pins the traveling front at a fixed  $x$ -coordinate. This is performed by a “pinning-shift” operator, which we denote  $\mathcal{P}$ . Our coarse time stepping is then modified from (7) to

$$\mathbf{v}^{n+1} = \mathcal{P} \mathcal{M} \{ \mathcal{T}_T \mu_j \} \Pi \mathbf{v}^n =: G(\mathbf{v}^n). \quad (11)$$

This formulation has a steady state at the constant shape moving front.

Let us start from the basic, Fourier based, pinning-shift operator  $\mathcal{P}^f : \mathbb{R}^M \rightarrow \mathbb{R}^M$ . After introducing a template function  $S(x)$ , we define

$$\mathcal{P}^f \mathbf{w} := \mathcal{S}_c^f \mathbf{w}, \quad c = \arg \max_{c' \in \mathbb{R}} \int_0^L (\Pi^f \mathbf{w})(x + c') S(x) dx. \quad (12)$$

Hence,  $\mathcal{P}^f \mathbf{w}$  is the shifted version of  $\mathbf{w}$  that best fits the template  $S(x)$ , in the sense that it maximizes the  $L_2$ -inner product between its Fourier interpolant and  $S$ . Upon convergence, the effective front speed  $v$  can be deduced from the converged value of  $c$  and the time reporting horizon  $T$  simply by taking  $v = c/T$ . With the template  $S(x) = 1 - \cos(2\pi x/L)$  we can compute the inner product in (12) explicitly,

$$\frac{1}{L} \int_0^L (\Pi^f \mathbf{w})(x + c') S(x) dx = \hat{w}_0 - \Re(\hat{w}_1 e^{ic'}) , \quad (13)$$

where  $\hat{w}_k$  are the Fourier coefficients of  $\mathbf{w}$ . Hence, since  $\hat{w}_0$  is real  $c$  in (12) should be chosen such that  $\hat{w}_1 e^{ic}$  is real and negative. This is easily implemented numerically together with the Fourier shift  $\mathcal{S}_c^f$ .

For the same reasons as in the implementation of the coarse time stepper, we would like to avoid direct Fourier interpolation of the solution, since it is not periodic. Therefore, we modify  $\mathcal{P}^f$  to operate on differences instead. In the same spirit as in Section 3.1, we let

$$\mathcal{P} := C \mathcal{P}^f D ,$$

with  $C$  and  $D$  defined in (10). We still use the effective propagation speed given by  $\mathcal{P}^f$ .

An important property of the Fourier based pinning shift operator is that it satisfies  $(\mathcal{P}^f)^2 = \mathcal{P}^f$ , which follows from the sampling theorem [12]. For other types of interpolation, such as piecewise polynomial interpolation, the pinning shift operator will not have this property and a steady moving coarse shape may not translate into a fixed point for (11). Our modification still has this property though, since

$$\mathcal{P}^2 = C \mathcal{P}^f D C \mathcal{P}^f D = C (\mathcal{P}^f)^2 D = C \mathcal{P}^f D = \mathcal{P} ,$$

where we used the fact that  $DC = I$ .

### 3.3 The RPM with pseudo-arclength continuation

RPM is an iterative procedure which can accelerate the location of fixed points of processes; under certain conditions it can help locate steady states of dynamic processes (in particular, discretized parabolic PDEs). It can be an acceleration technique for the solution of nonlinear equations, and a stabilizer of unstable numerical procedures (as it was first presented, [10]). Consider the fixed point problem

$$F(u; \lambda) = u , \quad (14)$$

and let  $J$  be the Jacobian of  $F$ .

- Like the Newton method, RPM can converge rapidly to the fixed point solution  $u^*$  provided the initial guess is good enough; the convergence occurs even if  $J(u^*)$  has a few eigenvalues larger than one. The computational

cost and convergence rate depend on the eigenvalues of  $J$ . Optimally there should be a clear gap in the spectrum between small and large (near the unit circle) eigenvalues and a limited number of large (in norm) eigenvalues for RPM to perform well.

- $J$  never needs to be evaluated directly, only  $F$ . We can therefore apply RPM to any “black box” code that defines a function  $F$ ; it is a “matrix-free” method.
- As a by-product, RPM also computes approximations of the largest eigenvalues of  $J$ . This gives approximate stability information about the fixed point.

When RPM is used for the computer-assisted bifurcation analysis of steady states of (usually dissipative evolution) PDEs, the function  $F$  represents a *time-stepper*: a subroutine that takes initial data and reports the solution of the PDE after some fixed time (the reporting horizon  $T$ ). A fixed point then satisfies (14). The conventional way of finding the steady state using a time-stepper would be to call it many times in succession—in effect, to integrate the PDE for a long time, corresponding to solving (14) by simple fixed point (Picard) iteration.

RPM can improve this approach in two important respects. First, the convergence can be significantly accelerated. The nature of many transport PDEs usually encountered in engineering modeling (the action of viscosity, heat conduction, diffusion, and the resulting spectra) dictates that there exists a separation of time-scales, which translates into an eigenvalue gap in the spectrum of  $J$  at the steady state. Second, RPM converges even if the steady state is slightly unstable, i.e. when  $J$  has a few eigenvalues outside the unit circle. It may thus be possible to compute (mildly) unsteady branches of the bifurcation diagram using forward integration (but in a non-conventional way, dictated by the RPM protocol). RPM still retains the simplicity of the fixed point iteration, in the sense that no more information is needed than just the time-integration code. This code, which may be a legacy code, and can incorporate the best physics and modeling available for the process, is used by RPM as a black box.

RPM can be seen as a modified version of fixed point iteration. It adaptively identifies the subspace corresponding to large (in norm) eigenvalues of  $J$ , hence the directions of slow or unstable time-evolution in phase space. In these directions the fixed point iteration is replaced by (approximate) Newton iteration. More precisely, suppose  $F : \mathbb{R}^N \times \mathbb{R} \rightarrow \mathbb{R}^N$  in (14). Let  $\mathbb{P}$  be the maximal invariant subspace of  $J$  corresponding to the  $m$  largest eigenvalues and let  $\mathbb{Q}$  be its orthogonal complement in  $\mathbb{R}^N$ . The solution  $u$  is decomposed as  $u = p + q = Pu + Qu$ , where  $P$  and  $Q$ , are the projection operators in  $\mathbb{R}^N$  on  $\mathbb{P}$  and  $\mathbb{Q}$ . These are constructed from an orthogonal basis  $V_p$

$$\begin{aligned} P &= V_p V_p^T, \\ Q &= I - V_p V_p^T. \end{aligned}$$

In a pseudo-arclength continuation context the solution  $u = u(s)$  and  $\lambda = \lambda(s)$ , where  $s$  parameterizes the bifurcation curve. In addition to (14) we then use an

algebraic equation to be able to handle turning points,

$$S(u, \lambda, \Delta s) = \frac{\|u(s) - u(s - \Delta s)\|^2}{\Delta s} + \frac{|\lambda(s) - \lambda(s - \Delta s)|^2}{\Delta s} - \Delta s = 0, \quad (15)$$

where  $u(s - \Delta s)$  and  $\lambda(s - \Delta s)$  refers to the converged solution at the previous point on the continuation curve.

The solution is advanced using a predictor-corrector method. Via extrapolation from previous points  $u_i = u(s_i)$ ,  $\lambda_i = \lambda(s_i)$  and  $\Delta s_i = s_{i+1} - s_i$ , the predictor-solution is obtained. Comparing a first order extrapolation,

$$\begin{aligned} \lambda^* &= \lambda_i + \frac{\lambda_i - \lambda_{i-1}}{\Delta s_{i-1}} \Delta s_i, \\ u^* &= u_i + \frac{u_i - u_{i-1}}{\Delta s_{i-1}} \Delta s_i, \end{aligned}$$

with a second order extrapolation,

$$\begin{aligned} \lambda^{**} &= \lambda^* + \frac{1}{2} \frac{\lambda_i(1 - \gamma) - 2\lambda_{i-1} + (1 + \gamma)\lambda_{i-2}}{\Delta s_{i-1} \Delta s_{i-2}} \Delta s_i^2, \\ u^{**} &= u^* + \frac{1}{2} \frac{u_i(1 - \gamma) - 2u_{i-1} + (1 + \gamma)u_{i-2}}{\Delta s_{i-1} \Delta s_{i-2}} \Delta s_i^2 \\ \gamma &= \frac{\Delta s_{i-1} - \Delta s_{i-2}}{\Delta s_{i-1} + \Delta s_{i-2}}, \end{aligned}$$

and requiring that

$$\max(\|u^{**} - u^*\|, |\lambda^{**} - \lambda^*|) < \epsilon \quad (16)$$

the stepsize is determined. Here  $\epsilon$  is a user specified tolerance. As the corrector method, we use RPM with pseudo-arclength continuation, see [10, 30]. Starting from  $u^0 = u^{**}$  and  $\lambda^0 = \lambda^{**}$ , the iterative scheme is given by

$$\begin{aligned} q^{n+1} &= QF(u^n, \lambda^n), \\ \begin{bmatrix} (V_p^T J V_p - I) & V_p^T F_\lambda \\ S_u^T V_p & S_\lambda \end{bmatrix} \begin{bmatrix} \Delta p \\ \Delta \lambda \end{bmatrix} &= - \begin{bmatrix} V_p^T F(p^n + q^{n+1}, \lambda^n) - p^n \\ S(p^n + q^{n+1}, \lambda^n) \end{bmatrix}, \\ u^{n+1} &= p^n + V_p \Delta p^n + q^{n+1}, \\ \lambda^{n+1} &= \lambda^n + \Delta \lambda^n, \end{aligned}$$

where the left hand side consists of partial derivatives of  $S$  in (15) and of  $F$  in (14) with respect to  $u$  and  $\lambda$ . The iterates  $u^n = p^n + q^n$  will converge to the solution of (14) under the assumptions discussed above. If the number of large norm eigenvalues,  $m$ , is limited, the dimension of  $\mathbb{P}$  and the projected Jacobian in the Newton iteration,  $V_p^T J V_p - I$ , remains small. Only this small matrix needs to be inverted. For a more complete description of RPM we refer to [10].

## 4 Numerical Results

In this section we present some numerical results using the coarse time stepper and the procedure described above to simulate an effective equation for the discrete problem in (8). We will start by discussing the “exact” bifurcation diagram of the discrete system, which we attempt to approximate. We will then show results obtained through the coarse time stepper, and discuss the effect of time stepper “construction parameters” like the reporting time horizon,  $T$  (the time to which (1) is integrated within the coarse time stepper), and the number of different initial shifted copies,  $N_c$ .

Figure 5 shows the bifurcation diagram of the discrete problem as a function of the parameter  $\Delta x$ , the lattice spacing, in the regime close to the onset of pinning. For lattice spacings smaller than  $\Delta x^* \approx 2.3$  the system has, as we discussed, an attracting, front-like solution that travels; its motion is *modulated* as it “passes over” the lattice points. For an infinite lattice, this modulated traveling solution possesses a discrete translational invariance:  $u_{\ell+1}(t + \tau) = u_{\ell}(t)$ . The shape of the modulating front is shifted by one (resp.  $2, 3, \dots, n$ ) lattice spacing after time  $\tau$  (resp.  $2\tau, 3\tau, \dots, n\tau$ ); this helps us define its effective speed  $v(\Delta x) \equiv \frac{\Delta x}{\tau}$  (see Figure 3). As  $\Delta x$  approaches zero, for an infinite lattice, the discrete front approaches the continuum front of the PDE, and its speed (the period of the modulation divided by  $\Delta x$  approaches the PDE front speed, 0.1 (see see Figure 3).

If we identify shapes shifted by one lattice constant, the attractor appears as a limit cycle with period  $\tau$ . As the lattice spacing approaches the critical value  $\Delta x^*$  the speed of propagation approaches zero (the period of the “limit cycle” approaches infinity); asymptotically,  $v(\Delta x) \approx |\Delta x - \Delta x^*|^{0.5}$ . As discussed in [20, 21] what occurs is a Saddle-Node Infinite Period (SNIPER) bifurcation: a saddle-node bifurcation where both new fixed points appear “on” the limit cycle. For larger values of  $\Delta x$  the “saddle” and the “node” move away from each other, and what used to be the limit cycle is now comprised from the saddle, the node, and both sides of the one-dimensional unstable manifold of the saddle, which asymptotically approach the node.

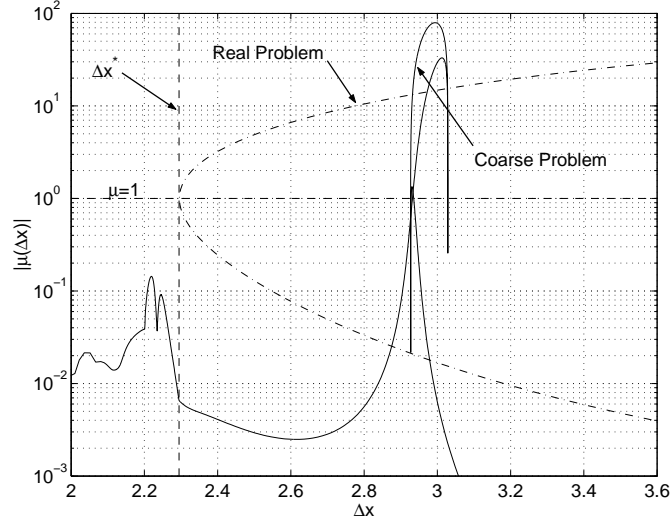
The saddle and the node are, of course, stationary fronts. A pair of them exists for every “unit cell”: all “node fronts” are shifts of each other by one lattice spacing, and all “saddle fronts” are also shifts of each other by one lattice spacing. Since the medium has a discrete translational invariance, this makes sense—if an initial condition gives rise to a front eventually pinned at some location in the discrete medium, the shift of this initial condition by one lattice spacing will eventually get trapped one lattice spacing further. This saddle-node bifurcation can be seen in Figure 5a; linearizing around the saddle front will give a positive eigenvalue  $\lambda_s$ , while the corresponding eigenvalue  $\lambda_n$  for the node front would be negative. Since we look at the problem in discrete time, what is plotted is the *multiplier*  $\mu_{n,s} = \exp(\lambda_{n,s}T)$ , where  $T$  is the reporting horizon. The saddle front has a multiplier larger than 1, while the corresponding multiplier for the stable node is less than 1; both multipliers asymptote to 1 at the SNIPER ( $\Delta x^*$ ).

Figure 5b shows the bifurcation diagram in terms of the front traveling speed. Since both the saddle and the node fronts are pinned (have zero speed) they both fall on the zero axis; we plotted their eigenvalues in Figure 5a to distinguish between them. The true traveling speed (broken line) is compared with the effective traveling speed predicted by a coarse time-stepper using  $N_c = 5$  copies within each unit cell, and a reporting horizon of  $T = 32$ . The coarse time stepper speed is a byproduct of fixed point computation and continuation with it; short bursts of detailed simulation are used in the RPM framework to construct a contraction mapping that converges to a fixed point of the time stepper. The final shift upon convergence (from the pinning-shift computation), divided by the time stepper reporting horizon gives us an estimate of the “effective speed”. Inspection of Figure 5b indicates that the coarse time stepper never predicts a speed that is exactly zero; yet it gives a good approximation of the effective speed, all the way from small  $\Delta x$  to the near neighborhood of the pinning transition, when the effective speed becomes small.

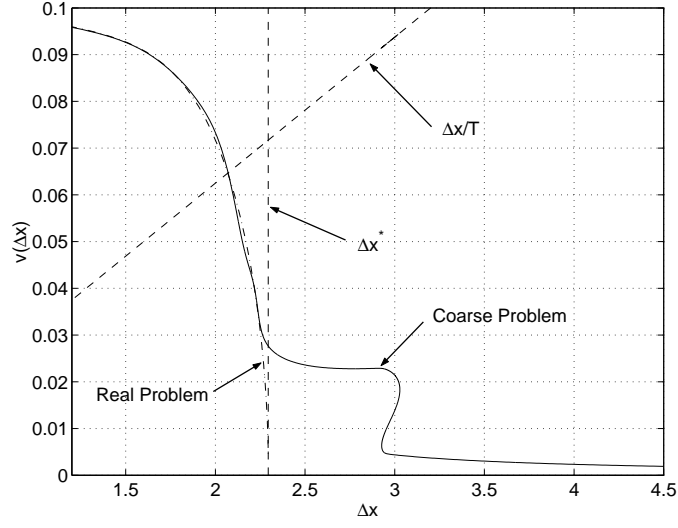
We will return to discussing this issue of “small residual motion” for the coarse time stepper shortly. To give an indication of when the procedure stops being quantitative, we have included the  $\Delta x/T$  curve in Figure 5b: disagreement starts well in the regime where the effective movement is *less* than one unit cell per observation period. In the next section we will compare the “goodness of approximation” of our coarse time stepper to the effective speed predicted by the Padé approach to extracting effective continuum equations. It is interesting that the coarse time stepper sometimes predicts a small hysteresis loop at low speeds, relatively close to “true pinning”; notice in Figure 5a the unstable (larger than one) multipliers for the brief saddle part of this loop. We will discuss a tentative rationalization of this below.

Figure 6 illustrates the effects of “time stepper construction” parameters on the effective behavior predicted by the time stepper: the reporting time-horizon, for two different sets of shifted copies ( $N_c = 3$  and  $N_c = 10$ ) as well as the effect of the number of copies for a fixed time horizon ( $T = 16$ ). Augmenting the time stepper reporting horizon is shown in Figure 6a-b; clearly, in both cases, extending the time stepper reporting horizon extends the region over which its effective speed agrees with the true problem closer to  $\Delta x^*$ . Larger numbers of copies ( $N_c = 5, 10, 20$ ) also perform slightly better than smaller numbers ( $N_c = 3$ ). In all cases the qualitative behavior is the same: (a) successful approximation of the effective speed until reasonably close to true pinning; (b) all differences occur when the average front motion is significantly less than one unit cell per reporting horizon; (c) there is always a slight residual motion, which—possibly after a small hysteresis loop close to true pinning—eventually becomes negligible.

We now turn to the discussion of the slight residual motion of the coarse time stepper at large  $\Delta x$  beyond  $\Delta x^*$ . For an infinite domain, the saddle and node pinned fronts appearing there are invariant to translations by one lattice spacing; for a large enough computational domain we still see two pinned front solutions per cell. When we “sprinkle” initial conditions along the cell, depending on their location with respect to the saddle front, the trajectories may either be attracted



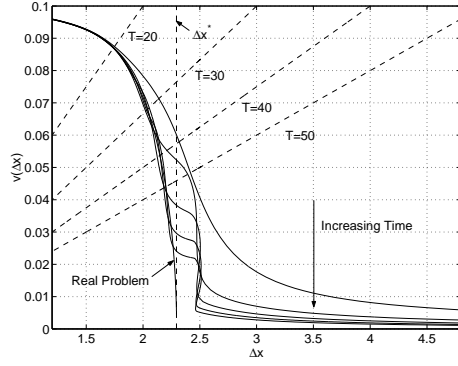
(a) Multipliers versus  $\Delta x$



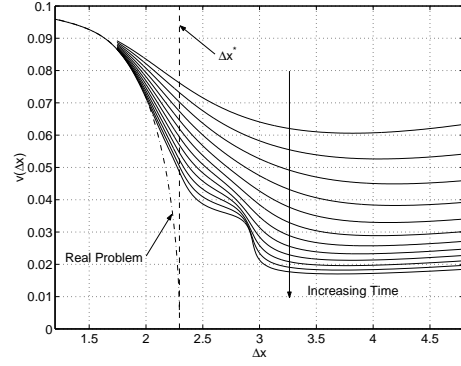
(b) Effective front speed versus  $\Delta x$

Figure 5: Detailed bifurcation diagram and coarse time stepper bifurcation diagram with parameters  $N_c = 5$ ,  $T = 32$ .

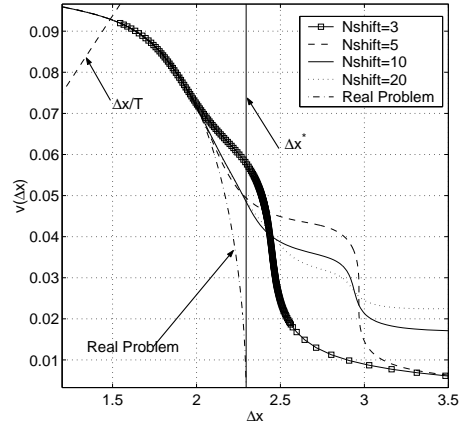




(a) Varying time horizon,  $T = 10, \dots, 50$ , with fixed  $N_c = 3$ . Dashed lines show  $\Delta x/T$ , i.e. speed required to traverse one cell.



(b) Varying time horizon,  $T = 5, \dots, 16$ , with fixed  $N_c = 10$ .



(c) Varying number of copies,  $N_c = 3, 5, 10, 20$ , with fixed  $T = 16$ .

Figure 6: Effective front speed versus  $\Delta x$  and the effect of varying the time horizon  $T$  and the number of copies  $N_c$ .

to the stable node “to the right” or to the one “to the left” of the saddle. It is instructive to represent these solutions as in Figure 7a, in a way that identifies the “right” node front with the “left” one; here translation along the lattice corresponds roughly to rotation along the circle. The node is denoted by a black circle, and the saddle by a white one. The small squares represent the initial positions of our initial condition “copies”. The fate of our distribution of initial conditions is governed by their initial “angle” on the circle—as our time horizon grows all initial conditions will asymptote to a stable front, either the left one (moving counterclockwise on the circle) or the right one (clockwise movement). We now see clearly the physical reason behind the net residual motion for any finite time horizon for the coarse time stepper. An initial condition that is put down “at random” in a unit cell deep in the pinned regime, even if it never exits this unit cell, will gradually traverse the part of the circle separating it from the closest node front.

When the critical parameter value is approached from the pinned side, the saddle and the node fronts approach each other on the circle, on their way to coalescing at the SNIPER bifurcation point [20, 21]. Figure 7b shows how this process becomes manifest in the coarse time stepper computations, using the problem in Figure 5 as our example. Deep in the pinning regime (high  $\Delta x$ , marked  $\alpha$ ) the relative “phase” of the saddle and the node pinned fronts on the circle remains roughly constant. The distance each member of our ensemble of initial conditions has traversed during one time horizon can be deduced from Figure 7b: the copy with the largest negative movement is the one closest to the saddle but on its left (copy number two). One can similarly rationalize the labelling of the remaining curves in Figure 7b. When  $\Delta x$  is reduced approaching the onset of pinning, at some point the saddle front starts moving appreciably towards the node front. As part of this movement, it “sweeps” the circle counterclockwise; at  $\Delta x \approx 2.8$  it has its first encounter with one of our initial conditions—the closest one on the left. When the saddle “moves past” it into the regime marked  $\beta$ , this copy, which was responsible for the largest negative displacement now approaches asymptotically the node front on the right, performing the largest *positive* displacement (and so on for the remaining copies). Eventually, in the propagating regime, marked  $\gamma$ , and for long enough reporting horizons, the initial “phase” difference (a fraction of a cell) becomes negligible compared to the net displacement of each point (several cells).

The real movement in phase space is shown in Figure 7c for two different  $\Delta x$ . In these subfigures, the  $x$ -axis represents  $\sin(2\pi x_c)$  where  $x_c$  corresponds to the location of the front, more specifically  $x_c = \sum_{\ell} (D\mathbf{u})_{\ell} \ell$ . The  $y$ -axis represents  $\max_{\ell} |(D\mathbf{u})_{\ell}|$ . The initial positions of the copies are indicated by small squares and their locations at  $t = T$ , the time horizon, are marked by filled circles. The labels refer to the same copies as in Figure 7b.

As the reporting time horizon of the time stepper goes to infinity, it is clear that one can compute the average residual movement from the asymptotic position of the saddle front, i.e. from the relative extent of the circle “to the right” and “to the left” of the saddle front. The most reasonable point to “declare” as an estimate of the true pinning from coarse time-stepper computations would

come from a polynomial extrapolation of the “successful” regime (close to the tip of the “apparent parabola” in Figure 5); alternatively, a value of  $\Delta x$  where the speed is small enough (well below one unit cell per time horizon) and its variation with number of copies and time horizon is below a user-prescribed tolerance, would also serve this purpose. While there is no well defined pinning bifurcation for the coarse time stepper (since pinning is an inherently non-translationally invariant bifurcation), the procedure can provide a good approximation of the effective shape and speed of the traveling fronts, as well as “common sense” ways of numerically estimating the true pinning.

## 5 An Alternative Continuum Approach: Padé Approximations

In this section, we propose an alternative scheme for capturing effects of discreteness, by means of a (now explicit) continuum equation. This PDE is obtained by means of Padé approximations [22, 23] which can be used to approximate discreteness in a quasi-continuum way, through the use of pseudo-differential operators. In particular, starting from the Taylor expansion for analytic functions, see e.g., [24],

$$u(x + m) = \exp(m\partial_x)u(x),$$

one can then express spatial discreteness as

$$\begin{aligned} u_{\ell+1} + u_{\ell-1} - 2u_\ell &\equiv (\exp(\Delta x\partial_x) + \exp(-\Delta x\partial_x) - 2)u(x) \\ &\equiv 4\sinh^2\left(\frac{\Delta x\partial_x}{2}\right)u(x, t). \end{aligned}$$

Expanding  $\exp(\pm\Delta x\partial_x)$  [23], one then obtains

$$\exp(\pm\Delta x\partial_x) - 1 = \frac{1}{2}\Delta x^2(1 + \frac{\Delta x^2}{12}\partial_x^2 + \dots)\partial_x^2 \pm \Delta x(1 + \frac{1}{6}\Delta x^2\partial_x^2 + \dots)\partial_x$$

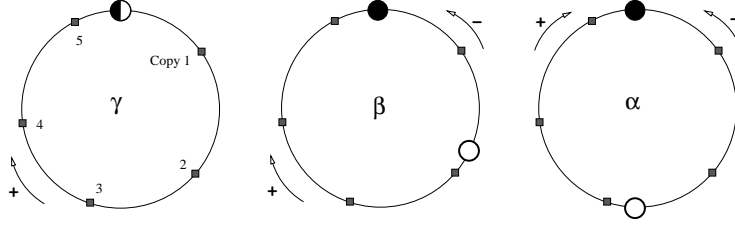
Finally, regrouping the terms in the manner of Padé [22, 23] yields

$$\exp(\pm\Delta x\partial_x) - 1 \approx \frac{1}{2} \frac{\Delta x^2\partial_x^2}{1 - \frac{\Delta x^2}{12}\partial_x^2} \pm \frac{\Delta x\partial_x}{(1 - \frac{\Delta x^2}{12}\partial_x^2)^2} \quad (17)$$

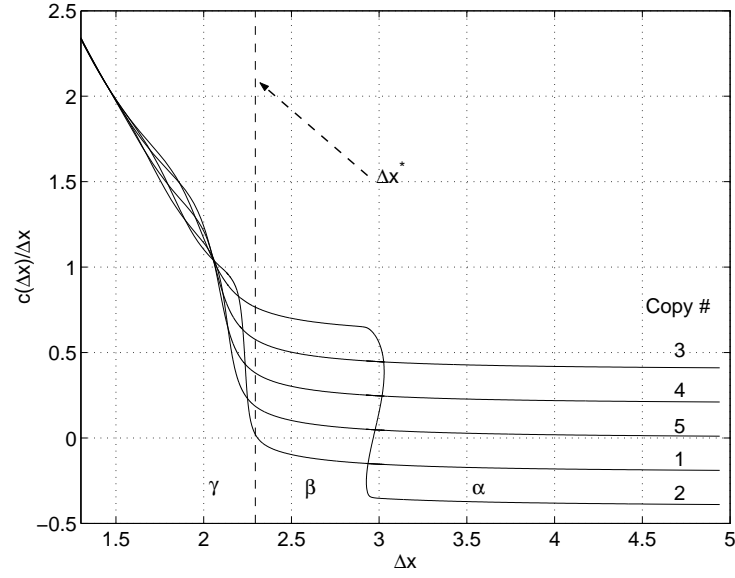
We now use the pseudo-differential operator approximation in (17) to convert the discrete model in (8) into the PDE approximation of the form:

$$u_t = \frac{\partial_x^2}{1 - \frac{\Delta x^2}{12}\partial_x^2}u + f(u). \quad (18)$$

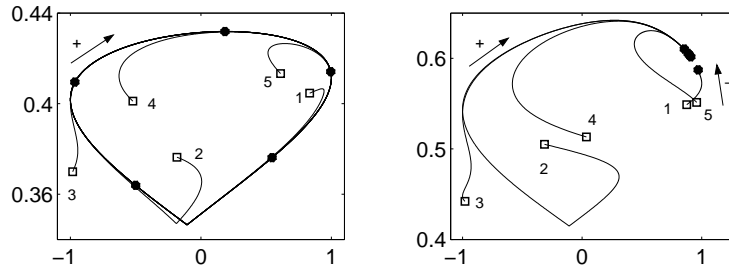
Such approaches were introduced and used extensively by Rosenau and collaborators [25, 26, 27] to regularize nonlinear wave equations, particularly of the Klein–Gordon type.



(a) Schematic movement of copies in phase space



(b) Distance traversed by copies



(c) Real movement of copies in phase space for  $\Delta x = 1.6$  (left) and  $\Delta x = 2.3$  (right). (See text for specification of axes.)

Figure 7: Movement of the individual copies, for  $N_c = 5$ ,  $T = 32$ .

Eq. (18) clearly emulates the discrete setting in some key aspects of the relevant spectral operator properties (i.e., of the discrete Laplacian in comparison with the pseudo-differential operator of (18)). For example, considering plane wave solutions of the form  $\exp(\lambda t - ikx)$ , we obtain in the discrete case the linearized dispersion relation (around a uniform state  $u = u_{\text{hom}}$ )

$$\lambda = \frac{2}{\Delta x^2} (\cos(k\Delta x) - 1) + f'(u_{\text{hom}}).$$

In the case of (18), the corresponding equation becomes

$$\lambda = -\frac{k^2}{1 + \frac{\Delta x^2}{12}k^2} + f'(u_{\text{hom}}).$$

Apart from sharing the continuum limit, the two dispersion relations share another qualitative feature which is particularly important [25, 26, 27]; namely, the presence of a lower bound in the continuous spectrum. Notice, however, that the two lower bounds are different ( $f'(u_{\text{hom}}) - 4/\Delta x^2$  in the discrete case versus  $f'(u_{\text{hom}}) - 12/\Delta x^2$  in the Padé approximation).

It would then be of interest to alleviate this spectral discrepancy, as well as to match the discrete operator (if possible) to a higher order in the Taylor expansion

$$\frac{u_{n+1} + u_{n-1} - 2u_n}{\Delta x^2} = \sum_{j=1}^{\infty} \frac{2\Delta x^{2j-2}}{(2j)!} u^{(2j)} = u_{xx} + \frac{\Delta x^2}{12} u_{xxxx} + \frac{\Delta x^4}{360} u_{6x} + O(\Delta x^6).$$

This can be achieved by a natural generalization in the form of a continued fraction such as e.g.,

$$\frac{\partial_x^2}{1 - \frac{A\partial_x^2}{1 - \frac{B\partial_x^2}{1 - C\partial_x^2}}}. \quad (19)$$

In order to use (19) in practice (i.e., for computational purposes), we convert the three fractions into one of the form

$$\frac{\partial_x^2(1 + \alpha\Delta x^2\partial_x^2)}{1 + (\alpha + \beta)\Delta x^2\partial_x^2 + \gamma\Delta x^4\partial_x^4}, \quad (20)$$

where a simple (algebraic) reduction of  $A, B, C$  to  $\alpha, \beta, \gamma$  has been used. We then use Taylor expansion of the denominator to convert the expression of (20) into one resembling (19). By matching up to  $O(h^6)$  the exact Taylor expansion, we obtain three algebraic equations for  $\alpha, \beta$  and  $\gamma$ . In this way, we obtain a set of solutions for  $\alpha, \beta$  and  $\gamma$ . We use here the set  $\alpha = -0.007\,912$ ,  $\beta = -1/12$ ,  $\gamma = 0.002\,056$ . An additional benefit (to the matching of the Taylor expansion up to correction terms of  $O(h^8)$ ) that should be highlighted here is the value  $\alpha/(\gamma\Delta x^2) = 3.848/\Delta x^2$  of the lower bound expression for  $\lambda$ , which is much closer to the theoretical lower bound of  $4/\Delta x^2$  than the prediction  $12/\Delta x^2$  of

the leading order approximation presented previously. The resulting evolution equation will then read:

$$u_t = \frac{\partial_x^2(1 + \alpha\Delta x^2\partial_x^2)}{1 + (\alpha + \beta)\Delta x^2\partial_x^2 + \gamma\Delta x^4\partial_x^4} + f(u) \quad (21)$$

Both (18) and (21) can be numerically implemented in a straightforward manner, by means of the spectral techniques described in [28]. We have performed numerical simulations of the front propagation, using 1024 modes in the spectral decomposition of (18) and (21). We will refer to these equations as the (Padé) models A and B respectively. A fourth order Runge–Kutta algorithm has been used for the time integration. For each value of  $\Delta x$ , we identify the position  $x_c$  of the front as the point where the ordinate of the front acquires the value  $u = 1/2$ . The linear interpolation scheme suggested in [29] has been implemented and has proved to be an efficient front tracking algorithm in all the examined cases.

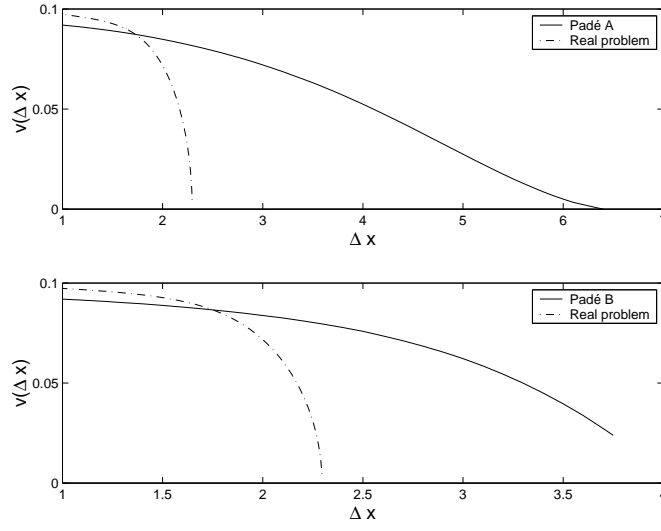


Figure 8: Effective front speed as a function of  $\Delta x$ , for the Padé model A (top panel) and model B (bottom panel).

Our results of this quasi-continuum approach to the discrete problem can be summarized in Figure 8 and Figure 9. Figure 8 shows the speed of the fronts in Padé models A and B respectively. We can observe that the critical value of  $\Delta x$  beyond which trapping of the front occurs is significantly displaced from the actual one of  $\Delta x^* \approx 2.3$ , for  $\eta = 0.45$ . In particular, for model A,  $\Delta x^* \approx 6.4$ , while for model B, the corresponding critical value is  $\Delta x^* \approx 3.8$ . We can deduce that the latter model is closer to the actual physical reality, even though the relevant prediction is still considerably higher than its actual value for the discrete model.

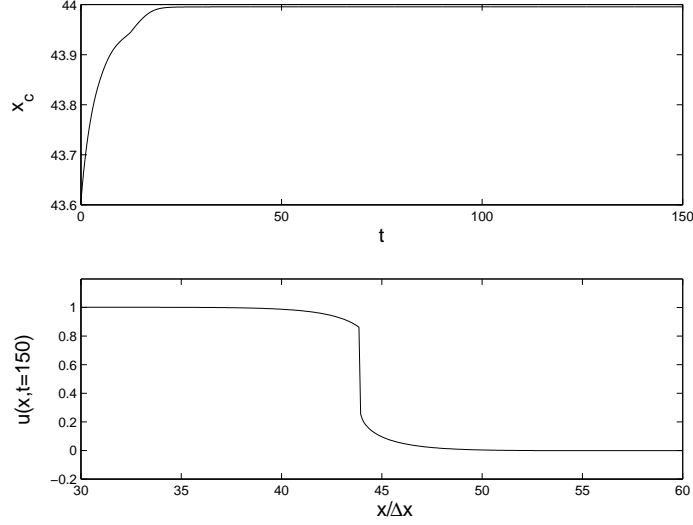


Figure 9: The figure shows the time evolution of the front for model A and for  $\Delta x = 6.4$ . The top panel shows the time evolution of the front center which eventually leads to trapping. The bottom panel shows the final front configuration of the numerical simulation at  $t = 150$ .

In part at least, these results (and the discrepancy from the actual discrete case) can be justified by observing Figure 9. The bottom panel of the figure suggests that the *only* way in which the front can stop in these quasi-continuum Padé approximations is by becoming practically a vertical shock-like structure. In this case, the “mass” of the front which is given by  $\int_{-\infty}^{\infty} u_x^2 dx$  (see e.g., [29] and references therein) becomes practically infinite. This means that the inertia of the front becomes too big for the front to move and hence “pinning” occurs. However, notice that this process of pinning is significantly different than the details of the discrete structure of the problem (such as e.g., the saddle-node bifurcation and the transition to pinned solutions). The translationally invariant quasi-continuum Padé approximations of models A and B do not “see” such features. Instead, they incorporate the well-known feature of front steepening for stronger discreteness [15] and the criticality of the latter feature eventually leads to pinning.

An additional pointer to the fact that such (pseudo-differential operator) models are “eligible” to pinning is that they are devoid of some of the important symmetries that are inherently related to traveling such as the Galilean invariance in the case of continuum bistable equation or the Lorentz invariance of its Hamiltonian (nonlinear Klein-Gordon) analog.

## 6 Summary and Discussion

We presented a computer-assisted approach for the *solution* of effective, translationally invariant equations for spatially discrete problems without deriving these equations in closed form. Assuming that such an equation exists, its time-one map is approximated through the coarse time stepper, constructed through an ensemble of appropriately initialized simulations of the detailed discrete problem. Combining the coarse time stepper with matrix-free based numerical analysis techniques, e.g. contraction mappings such as RPM, can then help analyze the unavailable effective equation. We are currently exploring the use of our coarse time stepper with coarse projective integration [13, 11, 31]. Matrix-free eigenanalysis techniques should also be explored, especially since they can help test the “fast slaving” hypothesis underlying the existence of a closed effective equation (see, for example, the discussion in [32, 33]).

We also presented initial computational results exploring the effect of certain “construction parameters” of the approach: the number of shifted copies in the ensemble of initial conditions, as well as the time-horizon used. We included a comparison between our approach and a particular way of obtaining explicit approximate translationally invariant evolution equations for such a problem (the Padé approximation). More work is necessary along these lines, exploring the relation of our approach with traditional homogenization methods at small lattice spacings. A discrete problem whose detailed solution can be obtained explicitly (perhaps a piecewise linear kinetics problem) or at least approximated very well analytically over short times, would be the ideal context in which to study these issues.

Several extensions of the approach can be envisioned, and might be interesting to explore. A time stepper based approach can be applied without modification to hybrid discrete-continuum media, e.g. continuum transport with a lattice of sources or sinks, such as cells secreting ligands into and binding them back from a liquid solution, [34]. It is clear that it can be tried in more than one dimensions, and for regular lattices of different geometry. For irregular lattices the averaging “over all shifts” we performed here for periodic media can be substituted with a Monte Carlo sampling over the distribution of possible lattices that takes into account what we know about the statistical geometry of the lattices. In this paper we assumed that an equation existed and closed for the *expected shape* of the solution. Conceivably one can attempt to develop time steppers not only for the expectation (the first moment of a distribution of possible results), but, say, for the expectation *and* the standard deviation of possible results; the lifting operator would then have to be appropriately modified. Finally, our time stepper here was built on short simulations of the *entire* detailed discrete system in space. Hybrid simulations, where a known, explicit effective equation is accurate over *part* of the physical domain can be done; an “overall hybrid coarse” time stepper (explicit equation over part of the domain, and the coarse time stepper in this paper over the rest of the domain) will then be used. In a multiscale context, we have proposed “gaptooth” and “patch dynamics” simulations [35, 36], where the present coarse time stepper integrations are per-



formed not over the entire domain, but over a mesh of small computational “boxes”. Both hybrid and “gaptooth” simulations, if possible, require careful boundary conditions for the “handshaking” between the continuum equation and the discrete simulations, or the discrete simulations in distant boxes, effectively implementing smoothness of the solution of the unavailable effective equation (e.g [36, 37, 38, 39, 40]).

We close with a discussion of the “onset of pinning”, the transition around which our test example of the coarse time stepper was focused. Continuum effective equations such as the ones discussed here through the numerical time-stepping procedure do *not*, strictly speaking, possess a bifurcation at the critical point of the genuinely discrete problem. In this effective process, the bifurcation is smeared out and rendered a “continuum transition” (see, for example, materials science models of the onset of movement of a front, [41, 42]). On the other hand, one might argue that this is an acceptable, and possibly optimal way for a continuum equation to represent the discrete bifurcation to pinning. We can see that other procedures, such as the discreteness-emulating Padé type ones, lose a lot of the quantitative structure of the relevant transition. On the other hand, if a continuum *differential* (as opposed to pseudo-differential) equation was constructed to “model” this transition, the latter would possess other artificial features such as a topologically mandated, unstable branch of traveling wave solutions [43]. It is conceivable that the short hysteresis loop sometimes predicted by the coarse time stepper close to pinning conditions is a “vestige” of this unstable branch that translationally invariant equations would necessarily predict. In conclusion, it can be appreciated that genuinely discrete problems and continuum ones have inherent differences<sup>1</sup> that cannot be fully captured by emulating (or “summarizing”) the one context through the other. Nevertheless, the approach proposed here, combined with a “common sense” interpretation of its results with respect to the genuinely discrete problem, performs in a satisfactory way for the modeler, even for the “most different” features between discrete and continuum models.

## Acknowledgments

Part of the research for this paper was carried out while Olof Runborg held a post-doctoral appointment with the Program for Applied and Computational Mathematics at Princeton University, supported by NSF KDI grant DMS-9872890. Panayotis G. Kevrekidis gratefully acknowledges support from a UMass FRG, NSF-DMS-0204585 and from the Eppley Foundation for Research. Kurt Lust is a postdoctoral fellow of the Fund for Scientific Research—Flanders. This paper presents research results of the Belgian Programme on Interuniversity Poles of Attraction, initiated by the Belgian State, Prime Minister’s Office for Science, Technology and Culture. The scientific responsibility rests with its

---

<sup>1</sup>A similar example can be found in the comparison of discrete and *periodic* continuum problems, where the former ones possess a single permissible band of excitations, while the latter possess an infinity of such bands and hence allow for interband transitions [44].

authors. Ioannis G. Kevrekidis gratefully acknowledges the support of AFOSR (Dynamics and Control) and an NSF-ITR grant.

## References

- [1] S. P. Dawson, J. Keizer and J. E. Pearson, Proc. Natl. Acad. Sci. U.S.A., **96**, 6060 (1999).
- [2] J. P. Keener, J. Theor. Biol., **148**, 49 (1991).
- [3] J. P. Laplante and T. Erneux, J. Phys. Chem., **96**, 4931 (1992).
- [4] A. V. Ustinov, T. Doderer, I. V. Vernik, N. F. Pedersen, R.P Huebener and V. A. Oboznov, Physica D, **68**, 41 1993.
- [5] D. N. Christodoulides and R. I. Joseph, Opt. Lett. **13**, 794 (1988).
- [6] B. L. Swanson *et al.* Phys. Rev. Lett., **82**, 3288 (1999).
- [7] J. Rinzel, D. Terman, X.-J. Wang and B. Ermentrout, Science, **279**, 1351 (1998)
- [8] D. McLaughlin, R. Shapley, M. Shelley and D. J. Wielaard Proc. Natl. Acad. Sci. USA **97** 8087 (2000)
- [9] M. Peyrard and A. R. Bishop, Phys. Rev. Lett., **62**, 2755 (1989).
- [10] G. M. Shroff and H. B. Keller, SIAM J. Numer. Anal. **30**, 1099 (1993).
- [11] C. W. Gear, I. G. Kevrekidis and C. Theodoropoulos, Comp. Chem. Engng. **26** 941 (2002); also I. G. Kevrekidis *et al.*, physics/0209043
- [12] O. Runborg, C. Theodoropoulos and I. G. Kevrekidis, Nonlinearity, **15**, 491 (2002).
- [13] C. W. Gear and I. G. Kevrekidis, SIAM J. Sci. Comp. **24** 1091 (2003).
- [14] Y. Ishimori and T. Munakata, J. Phys. Soc. Jpn. **51**, 3367 (1982).
- [15] M. Peyrard and M. D. Kruskal, Physica D **14**, 88 (1984).
- [16] J. P. Keener, Physica D **136**, 1 (2000).
- [17] G. Fath, Physica D **116**, 176 (1998).
- [18] C. W. Rowley and J. E. Marsden, Physica D, **142**, 1 (2000).
- [19] L.-Y. Chen and N. Goldenfeld, Phys. Rev. E, **51** 5577 (1995)
- [20] P. G. Kevrekidis, I. G. Kevrekidis and A. R. Bishop, Phys. Lett. A **279**, 361 (2001).

- [21] A. Carpio and L. L. Bonilla, SIAM J. Appl. Math. **63**, 1056 (2003); A. Carpio and L.L. Bonilla, Phys. Rev. E **67**, 056621 (2003).
- [22] Padé approximants Method and its Applications to Mechanics, H. Cabannes (ed.), Springer-Verlag, Berlin (1976).
- [23] C. Elphick, E. Meron and E. A. Spiegel, SIAM J. Appl. Math. **50**, 490 (1990).
- [24] P. L. Christiansen, Y. G. Gaididei, F. G. Mertens and S. F. Mingaleev, Eur. Phys. J. B **19**, 545 (2001).
- [25] P. Rosenau, Phys. Lett. A **118**, 222 (1986).
- [26] P. Rosenau, Phys. Rev. B **36**, 5868 (1987).
- [27] P. Rosenau, Phys. Rev. A **40**, 7193 (1989), *ibid.* **46**, R7371 (1992); C. R. Doering, P. S. Hagan and P. Rosenau, Phys. Rev. A **36**, 985 (1987).
- [28] P. G. Kevrekidis, I. G. Kevrekidis, A. R. Bishop and E. S. Titi, Phys. Rev. E **65**, 046613 (2002).
- [29] R. Boesch, C. R. Willis, and M. El-Batanouny, Phys. Rev. B **40**, 2284 (1989).
- [30] K. Lust, PhD Thesis, Katholieke Universiteit Leuven, (1997).
- [31] R. Rico-Martinez, C. W. Gear and I. G. Kevrekidis (2003) J. Comp. Phys., submitted; also nlin.CG/0307016 at arXiv.org.
- [32] A. G. Makeev, D. Maroudas and I. G. Kevrekidis, (2002) J. Chem. Phys. **116** 10083-10091.
- [33] G. Hummer and I. G. Kevrekidis (2003) J. Chem. Phys. **118**(23) pp. 10762-10773.
- [34] M. Pribyl, C. B. Muratov and S. Shvartsman (2003) Biophys. J. **84** pp.3624-3635.
- [35] C. W. Gear, J. Li and I. G. Kevrekidis (2003) Physics Letters A, *in press*; also physics/0303010 at arXiv.org
- [36] I. G. Kevrekidis, C. W. Gear, J. M. Hyman, P. G. Kevrekidis, O. Runborg and K. Theodoropoulos (2003) Comm. Math. Sciences, submitted; also physics/0209043 at arXiv.org.
- [37] J. Li, D. Liao and S. Yip (1998) *Phys. Rev. E* **57** 7259-7267
- [38] J. Li, D. Liao and S. Yip (1998) *Mat. Res. Soc. Symp. Proc.* **538** 473.
- [39] V. B. Shenoy, R. Miller, E. B. Tadmor, D. Rodney, R. Phillips and M. Ortiz (1999) J. Mechanics and Phys. Solids, **47**.

- [40] W. E and Z. Huang (2001) Phys. Rev. Letters **87** 135501.
- [41] J. W. Cahn (1962) Acta Metallurgica **10** pp.789-798.
- [42] D. Maroudas and R. A. Brown (1991) Appl. Phys. Lett. **88**(17) pp. 1842-1844.
- [43] See e.g., M. Kness, L.S. Tuckermann and D. Barkley, Phys. Rev. A **46**, 5054 (1992) and references therein.
- [44] G. L. Alfimov *et al.*, Phys. Rev. E **66**, 046608 (2002).